Natural Product P57 Induces Hibernation-like State through Targeting Pyridoxal Kinase

Yongjun Dang (yongjundang@fudan.edu.cn)
Fudan University https://orcid.org/0000-0001-7237-1132

Rui-Na Wang
Fudan University

Lei Xiao
Fudan University https://orcid.org/0000-0002-6897-4608

Jianpo Pan
Chongqing Medical University

Di Zhu
Fudan University

Jun Wang
Shanghai Institute of Materia Medica

Chengfeng Pei
Institute of Organic Chemistry, Chinese Academy of Sciences

Qinfeng Ma
Chongqing Medical University

Guangsen Bao
Fudan University

Ziruoyu Wang
Fudan University

Mengdi Zhu
State Key Laboratory of Drug Research, Shanghai Institute of Materia Medica, Chinese Academy of Sciences, Shanghai / University of Chinese Academy of Sciences, Beijing

Guoxiang Wang
Institutes of Brain Science & Collaborative Innovation Center for Brain Science; State Key Laboratory of Medical Neurobiology; Fudan University

Ling Gong
Fudan University

Qiuping Tong
Fudan University

Min Jiang
Fudan University

Junchi Hu

Chongqing Medicinal University

Miao He

Fudan University https://orcid.org/0000-0003-0731-6801

Yun Wang

Fudan University

Tiejun li

SMMU

Wei Li

China Pharmaceutical University https://orcid.org/0000-0003-0388-1467

Chun-Min Liang

Department of Anatomy and Histology and Embryology, Shanghai Medical College, Fudan University

Zengxia Li

Fudan University, School of Basic Medical Sciences

Dengke Ma

University of California, San Francisco https://orcid.org/0000-0002-5619-7485

Minjia Tan

Shanghai Institute of Materia Medica, Chinese Academy of Science https://orcid.org/0000-0002-6784-9653

Jun-Yan Liu

Chongqing Medical University https://orcid.org/0000-0002-3018-0335

Wei Jiang

Fudan University https://orcid.org/0000-0001-7615-0900

Cheng Luo

Shanghai Institute of Materia Medica https://orcid.org/0000-0003-3864-8382

Biao Yu

Institute of Organic Chemistry, Chinese Academy of Sciences

Article

Keywords:

Posted Date: April 28th, 2022

DOI: https://doi.org/10.21203/rs.3.rs-1518013/v1

Version of Record: A version of this preprint was published at Nature Communications on September 26th, 2023. See the published version at https://doi.org/10.1038/s41467-023-41435-y.

Abstract

Hibernation/torpor enables certain mammals to survive under extreme environmental conditions. However, pharmacological induction of hibernation-like or torpor state in most mammals remains a huge challenge. Here we show that a natural product P57 promptly induces hypothermia and decreases energy expenditure in rodents. Mechanistically, P57 inhibits the kinase activity of pyridoxal kinase (PDXK), a key metabolic enzyme of vitamin B6 catalyzing phosphorylation of pyridoxal (PL), resulting in the accumulation of PL in hypothalamus to cause hypothermia. The hypothermia induced by P57 is significantly recuperated in the mice with knockout of PDXK in medial preoptic area (MPA). We further found that P57 and PL have consistent effects on gene expression regulation in hypothalamus, and both directly activate MPA neurons to induce hypothermia. Taken together, our findings demonstrate that P57 has a potential application in therapeutic hypothermia through regulation of vitamin B6 metabolism and PDXK serves as a previously unknown target of P57 in thermoregulation. In addition, P57 may serve as a chemical probe for exploring the neuron circuitry related to hibernation-like state in rodents.

introduction

Many mammals enter hibernation/torpor in adaption to extreme environmental conditions. Hibernation or torpor is characterized by pronounced temporal reductions in body temperature and energy expenditure. Hibernation-capable mammals can develop resilience to ischemic stress and hypothermia in a therapeutic setting can protect human tissues from cell death in many neurovascular and cardiovascular ischemic diseases[1-8]. Whether and how small molecules pharmacologically induce hypothermia or hibernation-like state remains largely unknown. Eight classes of agents have been reported to have hypothermic and neuroprotective effects in preclinical ischemic models, including cannabinoids[9-12], transient receptor potential vanilloid 1 (TRPV1) agonists[13,14], opioid receptors agonists[15-20], neurotensin[21-25] and thyroxine derivatives[26,27]. However, these compounds are rarely used in clinics given undefined clinical efficacy, unclear mechanisms of action in neuroprotection and multiple side effects. It has been known that body temperature is tightly controlled by the preoptic area in hypothalamus, but the exact regulatory neurons and their connections have not been understood[28,29]. Therefore, compounds that specifically target temperature-sensitive neurons in hypothalamus may be useful not only in the clinic but also as tools to facilitate the investigation of mechanisms and circuitry involved in hibernation-like state.

Results

P57 induces a hibernation-like/torpor state in rodents

P57, an oxypregnane steroidal glycoside, is a well-known natural product isolated from *Hoodia gordonii* for its prominent activity of appetite suppression through undefined mechanism[30,31]. Upon completion of total synthesis of P57 (Fig. 1a), we began to study its potential functions in rodents. Serendipitously, we

observed that intraperitoneal injection of P57 caused a significant and reversible decrease in body core temperature by Anilogger core temperature monitoring system. Core temperature was reduced by approximately 2 to 5°C, lasting for 2 to 5 hours with a single dose of P57 at 12.5 mg/kg and 25.0 mg/kg, respectively (Fig. 1b). Mammals maintain body temperature by regulating metabolism, prompting us to investigate the metabolic changes induced by P57. Indeed, O_2 consumption, CO_2 production, respiratory exchange ratio (RER) and energy expenditure were all significantly decreased in P57-treated mice and returned back to baseline levels after around 7 hours (Fig. 1c, d and Fig.S1a, b). Same as the effect of natural P57[30,31], P57-treated mice had a substantial decrease in food intake (Fig.S1c). We further assessed the effect of P57 on mouse motor activity, and observed that travel distance in the open-field test and latency to fall in the rotarod test were significantly decreased with administration of P57 (Fig.S1d, e). Mouse motor behaviors also gradually returned to normal (Fig.S1d, e). These results indicate that P57 caused a hypothermic and hypometabolic state in a reversible manner.

A long-lasting hypothermic and hypometabolic state is similar to hibernation or daily torpor[32]. We further administrated 4 consecutive intraperitoneal injection to mice with 25.0 mg/kg of P57 every 3 hours and observed that the core temperature of mice could be as low as 26°C and the hypothermic state (T_{core}<34°C) lasted for longer than 30 hours with decreased activity (Fig. 1e). In addition, gross histological examination of brain, heart, kidney, liver and muscle did not show any damage after recovery (Fig.S1f). Hence, consecutive P57 treatments were able to induce a hibernation-like or torpor state.

Hypothermia or hibernation-like state has neuroprotective effects in ischemic diseases[33–36]. We found that the core body temperature in rats was also rapidly reduced from around 37.0°C to 34.0°C after P57 administration within 1 hour and the therapeutic hypothermia lasted for more than 4 hours in a dose-dependent manner (Fig.S2a). In a rat ischemic stroke model using middle cerebral artery occlusion (MCAO), P57 treatment obviously decreased infarct volumes (Vehicle: 29.9 ± 4.4% vs. P57: 11.9 ± 5.7%) (Fig.S2b, c). These results indicate that P57 can induce hibernation-like state in rodents and protect against ischemic injuries in the brain.

P57 binds with PDXK and inhibits its kinase activity

P57 is rapidly diffused to brain after the intravenous administration[37]. To explore the mechanism of P57, we synthesized a biotinylated probe of P57 (Fig. 2a), and identified its putative targets through affinity purification from mouse brain tissue lysates, followed by mass spec analysis of P57-bound proteins (Fig.S3a, table S1). Among the identified proteins, glutathione S-transferase P1 (GSTP1), pyridoxal kinase (PDXK) and neuromodulin were significantly enriched by Bio-P57. Further validation with immunoblotting showed GSTP1 and PDXK, but not neuromodulin, were sensitive to competition by excess P57 (Fig. 2b, Fig.S3b). GSTP1 was excluded as the potential physiological target of P57 since we did not observe any body temperature change when mice were treated with its inhibitors (ethacrynic acid or celastrol[38]) or agonist (α-angelica lactone), as well as the substrate (glutathione, GSH) of GSTP1 (Fig.S3c ~ e), leaving PDXK as the only remaining target candidate.

PDXK is responsible for the phosphorylation of vitamin B6, which includes pyridoxal (PL), the major form *in vivo*, pyridoxamine (PM) and pyridoxine (PN), in the presence of ATP and Zn^{2+} or Mg^{2+}. Phosphorylation of vitamin B6 constitutes an essential step in the synthesis of pyridoxine 5'-phosphate (PLP), the active form of vitamin B6 and a cofactor for over 160 enzymes. We further characterized P57 binding to PDXK by a pull-down assay using the purified recombinant PDXK protein and observed that binding of biotinylated P57 to PDXK was sensitive to competition by unmodified P57 (Fig. 2c). Microscale thermophoresis (MST) and surface plasmon resonance (SPR) revealed binding affinity between P57 and PDXK, with dissociation constants of 15.8 ± 2.9 μM and 3.5 μM, respectively (Fig. 2d, e).

We next determined whether kinase activity of PDXK was affected by P57. We found that P57 inhibited PDXK enzyme activity in a dose-dependent manner, with EC_{50} at 20.0 to 30.0 μM (Fig.S4a). Kinetic studies with P57 wherein ATP concentration was fixed and concentration of PL was varied showed that Vmax remained constant and Km values increased, which indicated that P57 competitively inhibited PDXK with PL (Fig. 2f, Fig.S4b). Similar experiments wherein PL concentration was fixed and the concentrations of ATP were varied showed that both K_m and V_{max} values decreased, indicating that P57 uncompetitively inhibits PDXK with respect to ATP (Fig.S4c).

To investigate how P57 might bind to PDXK, we used the ligand docking program Schrodinger Glide to dock P57 into the PLP binding pocket of PDXK (3KEU)[39]. The procedure was validated by redocking with a root mean square deviation (RMSD) of 0.125 Å between the docked conformation and co-crystallized pose. P57 could be docked into the PL-binding site in a PL competitive way (Fig. 2g, h). P57 is stabilized by hydrogen bonding interactions with Thr47, Gly232 and Asp235 residues at the active site. To further verify our docking model, we evaluated the inhibitory action of P57 with respect to PL. Compared with the PDXK binding in absence of PL, the apparent K_d for P57 against PDXK was dramatically reduced with increasing concentration of PL (Fig.S3f). Aglycone fragment of P57 showed a dramatically reduced affinity with PDXK (K_d=123.5 ± 35.4 μM) (Fig.S3g). Kinetic studies with P57-aglycone wherein PL concentration was fixed and the concentrations of ATP were varied showed that Km remained constant and Vmax values decreased, which indicated that P57-aglycone is a non-competitive inhibitor of PDXK (Fig.S4d). D235 and G232 jointly participate in the stabilization of the conformation at one terminal of P57. Accordingly, the D235A mutation can reduce the binding stability to a certain extent, and partly reducing the inhibitory activity. On the contrary, T47V mutation removes the hydrogen bond anchor on the other end, thereby increasing the flexibility of the tail, resulting in a complete loss of the inhibitory activity (Fig.S3h). Together, these results indicate that PDXK is a target of P57 and its kinase activity is inhibited by P57.

P57 mainly targets PDXK in hypothalamus to induces hypothermia

To determine whether hypothermia induced by P57 was mediated through PDXK inhibition *in vivo*, we measured vitamin B6 level in hypothalamus and whole mouse brain after 25.0 mg/kg of P57 treatment using a high-performance liquid chromatography spectrometry. PL level, but not other vitamin B6 forms

such as PN, PM and 4-PA, was dramatically increased in hypothalamus after intraperitoneal administration of P57, but there was no obvious change in whole brain tissues (Fig. 3a, table S2 and table S3), which suggests the hypothalamus as the effector region of P57-induced hypothermia. Pioneering studies have shown that the preoptic area (POA) of the hypothalamus plays a key role in thermoregulation and energy balance[40,41]. We thus locally administered P57 into POA at 0.6 mg/kg and 1.2 mg/kg respectively and observed rapidly induction of deeper hypothermia in a dose-dependent manner (Fig. 3b, c). However, the core temperature of mice didn't change when P57 was administrated directly into caudate putamen (CPu) (Fig.S5a, b). Moreover, we expressed Cre-eGFP in hypothalamus by injecting *Pdxk*$^{flox/flox}$ mice with AAV2/9-hSyn-Cre-EGFP-WPRE-pA, the effect of P57 (25.0 mg/kg) on inducing hypothermia was significantly reduced in the mice with knocking out PDXK in POA neurons compared to control group (Fig. 3d, e, Fig.S5c). As P57-induced inhibition of PDXK will dramatically increase the PL level in hypothalamus, we directly tested the effect of PL in hypothermia. We observed mouse core body temperature decreased to around 30.0°C after intraperitoneal administration of PL at 300.0 mg/kg, but other B6 vitamers could not change the core temperature at the same dosage (Fig. 3f, Fig.S5d). In addition, 5.0 mg/kg of PL administrated directly into POA rapidly induced hypothermia (Fig. 3g). Combined intraperitoneal administration of P57 (12.5 mg/kg) and PL (200.0 mg/kg) caused a synergistic reduction of body temperature (Fig. 3H). We also observed that travel distance in the open-field test and latency to fall in the rotarod test were significantly decreased with administration of PL (Fig.S5e, f). These results confirm that P57 inhibits the enzyme activity of PDXK to induce hypothermia through specifically increasing hypothalamus PL level.

P57 and PL play a similar effect on hypothalamus neurons

To further characterize the state of various cell types in the hypothalamus after administering P57 and PL respectively, and explore the mechanism of regulating core temperature, we performed single-nucleus RNA-sequencing (snRNA-seq) using nuclei dissociated from mouse hypothalamus. C57 wild-type mice were injected with P57 and PL respectively, while mice treated with phosphate buffered saline were included as control. A total of 40,008 single nuclei were analyzed after removing low quality cells and doublets. Unsupervised clustering analysis delineated the dominant neuronal and non-neuronal cells clusters. Glutamatergic and GABAergic neurons, the two most populated clusters (n = 21411), are further divided into neuronal subpopulation (24 glutamatergic and 15 GABAergic clusters) (Fig. S6, Fig.S7a). The changes of differentially expressed genes (DEGs) between P57 and PL show a similar pattern (Fig. 4a, c). We also found a significant positive correlation between P57 and PL in the DEGs (Pearson's correlation coefficient 0.86, P = 3.9e-12) and the number of cells in each cluster (Pearson's correlation coefficient 0.86, P = 1.6e-12) (Fig. 4b; Fig.S7b). These results indicate the significant similar effect on gene expression of neurons in hypothalamus with P57 and PL treatment.

We further statistically analyzed the overlapped DEGs between P57 and PL treatment in each cluster (Fig. 4d). The KEGG functional enrichment analysis on the intersection genes in cluster 12 and 13, the top two clusters in terms of ratio of overlapped DEGs between P57 and PL treatment, shows that GABAergic

synapse and glutamatergic synapse were significantly enriched (Fig.S7c, d). The third top cluster 6 is anatomically located in MPA according the Harmonizome database[42]. We selected the top 6 marker genes for MPA (Pbx1, Esr1, Uba1, Ndfip1, Tex22, Pgr), and found that these marker genes are highly expressed in clusters 4,6,7 and 10, suggesting that these clusters likely to contained a significant number of neurons from the MPA (Fig.S7e). Zhang et al reported that activating ERα$^+$ MPA neurons was sufficient to drive a torpor-like state in rodents[43]. For these clusters, we performed enrichment analysis for DEGs between P57/PL and control groups. Results shows that there was significant overlap in gene expression between P57 and PL in the MPA (Fig. 4e), and KEGG pathway analysis suggests both small molecules upregulate glutamatergic synapse and downregulate GABAergic synapse signaling pathways (Fig. 4f).

P57 and PL activate neurons in MPA to induce hypothermia

To investigate the effect of P57 and PL on the activities of MPA neurons during regulation of the core temperature, we monitored the expression of immediate early gene – c-Fos upon intraperitoneal administration of either P57 or PL. We observed three regions of marked activation of c-Fos in mice brain, that is MPA (Fig. 5a, b), bed nucleus of the stria terminalis, lateral division, dorsal part (BSTLD) (Fig.S8a, b) and paraventricular nucleus of hypothalamus (PVH) (Fig.S8a, c). We then directly recorded the activity of MPA neurons in slice with patch-clamp technique. Either P57 or PL application increased the firing rate of MPA neurons (Fig. 5c, d and Fig.S9a-c). Finally, with *in vivo* fiber photometry calcium signal recording, we simultaneously monitored the changes of MPA GABA or glutamate neuronal activity based on GCaMP and mouse core body temperature. GCaMP fluorescence signal from both GABA and glutamate neurons was increased with the falling of body temperature after intraperitoneal administration of P57 or PL (Fig. 5e-g and Fig.S9d, e). In addition, the fluctuation degree of GCaMP also increased with the reduction of core body temperature (Fig. 5f, g and Fig.S9d, e). Together with previous studies showing that increasing the activity of MPA GABA and glutamate neurons could reduce core body temperature[29,44,45], our results indicate that MPA is a core target of P57 for inducing hypothermia.

Discussion

In this study, we demonstrate that P57 robustly induces hibernation-like or torpor state in mice through targeting PDXK, the key enzyme of vitamin B6 metabolism (Fig. S10). P57 administration rapidly decreases core body temperature within minutes and the hypothermic state can be maintained by adjusting the drug dose. Hypothermic state induced by P57 shares several features with hibernation-like state and therapeutically induced hypothermia. First, consecutive treatment of P57 maintains the lengthy hypothermic state while the thermoregulatory system remains functional when the theoretical core temperature is lowered. Second, there is no tissue damage despite physiological functions being suppressed in hypothermic state. Third, animal is able to recover from P57-induced hypothermia without any external manipulation. In addition, we also find that P57 has remarkable neuroprotective effects in a rat MCAO model (Fig.S2b, c), indicating that P57 may act as a potent new therapeutic approach to treat ischemic diseases.

Target identification of natural products is one of the main bottlenecks in drug development. Previous studies showed that P57 significantly suppressed appetite activity and decreased body weight[31,46,47], but the underlying mechanisms are unclear, which is the one of limiting factors for its clinical application[37,46,47]. Identification of PDXK as the target of P57 (Fig. 2) provides insight into its mechanism of actions and will prompt structural optimization of P57 to be applied in clinical settings. Interestingly, P57 inhibits PDXK enzyme activity to specifically accumulate PL in hypothalamus (Fig. 2f and Fig. 3a), resulting in a rapid decrease in core temperature and basal metabolic rate. We do not exclude the possibility that mechanism of thermoregulation by P57 and PL is related to PLP, which is a cofactor for many metabolic enzymes, though it is unlikely because PL administration is sufficient to induce hypothermia (Fig. 3f, g, Fig.S5d). Defects of vitamin B6 metabolism in the brain leads to early onset of vitamin B6-dependent epilepsy refractory to anticonvulsants[48]. *PDXK* mutation leads to peripheral neuropathy with optic atrophy[49]. The mechanisms involved in these neurological diseases are largely unknown. P57 will be a useful tool to investigate PDXK and vitamin B6's function in these neuronal pathological processes.

Several neuronal subpopulations in POA are uncovered to directly regulate core body temperature, including glutamatergic LepRb neurons[50], *Trpm2*$^{+}$*/Vglut2*$^{+}$ POA neurons[51], VMPO$^{BDNF/PACAP}$ neurons[52], GABAergic neurons in the vLPO[29], ERα^{+} neurons in the MPA[43], Q neurons (encoding pyroglutamylated RF amide peptide, QRFP) within AVPe/MPA[45] and *Vglut2*$^{+}$*Adcyap1*$^{+}$ neurons[44]. Whether and how the information about core body temperature transmitted by these neurons is integrated remains to be understood. We found P57 and PL can activate neuronal subpopulations in MPA through evaluating c-Fos expression and the change of calcium signal (Fig. 5, Fig. S8 and S9). Moreover, we also observed c-Fos activation in PVH. PVH not only plays a crucial role in regulating neuroendocrine axes and energy balance, but also participates in core body thermoregulation[53–55]. The snRNA-seq results also showed the neurons in cluster 19 highly expressed Sim-1 were significantly activated, which gives a clue to further explored neurons affected by P57 in thermoregulation and appetite. However, the mechanism of how P57 and PL activate these neurons, directly via inhibition of PDXK or indirectly via hypothermia, remains to be investigated. Further explorations of the neuronal circuit participated in hypothermia induced by P57 and PL are worth investigating. Nonetheless, potent effects of P57 and PL demonstrate feasibility of pharmacological induction of therapeutic hypothermia or hibernation-like state in mammals. Furthermore, identification of PDXK as a target of P57 reveals previously unknown roles of vitamin B6 metabolism in thermoregulation and will offer an opportunity for future clinical drug development to control hypothermia or hibernation-like state and other related disease processes.

Methods

Data reporting

No statistical methods were used to predetermine sample size. Animals used were randomly assigned to groups before experiments and the investigators were not blinded to allocation during experiments and

outcome assessment.

Animals

All animal care and experimentation were ethically performed according to procedures approved by the Institutional Animal Care and Use Committee at Fudan University. Mice were housed 3–5 per cage (except in metabolic chamber in which mice were singly caged or preparing for core temperature detection) in a 12 h light/12 h dark cycle with ad libitum access to regular chow and water, and maintained at an ambient temperature of 23℃ and a relative humidity of 50%. We used 6 ~ 8-week-old WT male C57BL/6J mice (SLAC company), Wistar rats (SLAC company), Vglut2-ires-Cre (Jackson Lab), Vgat-ires-Cre (Jackson Lab). All mouse lines are in a WT (C57BL/6J) background.

Pdxk $^{flox/flox}$ mice were generated by CRISPR/Cas 9-mediated genome engineering. Exon2 of *Pdxk-201* (ENSMUST00000041616.14) transcript, containing 55 bp coding sequence, is recommended as the knockout region based on the structure of *pdxk*. In brief, sgRNA was transcribed in vitro, donor vector was constructed. Cas9, sgRNA and donor were microinjected into the zygotes of C57BL/6JGpt mice. Zygotes were transplanted to obtain positive F0 mice which were confirmed by PCR and sequencing. A stable F1 generation mouse model was obtained by mating positive F0 generation mice with C57BL/6JGpt mice.

Chemicals

P57[56] and its derivatives were kindly provided from Biao Yu's group by totally synthesized. Pyridoxal (PL, 322481) and pyridoxal 5'-phosphate (PLP, 303712) were obtained from J&K Scientific. Pyridoxamine (PM, P9380), pyridoxine (PN, P9755), 4-pyridoxic acid (4-PA, P9630), pyridoxal-(methyl-d3) (D3-PL, 705187), celastrol (cela, C0869), ethacrynic acid (EA, SML1083) and 2,3,5-triphenyltetrazolium chloride (TTC, 8877) were obtained from Sigma Aldrich. α-angelica lactone (HY-N0548) was obtained from MCE. Glutathione (GSH, 101814) was obtained from MP Biomedicals.

Viruses

AAV2/9-hSyn-DIO-jGCaMP7s (S0590-9), AAV2/9-hSyn-eGFP-WPRE-pA (S0237-9-H20), and AAV2/9-hSyn-Cre-eGFP-WPRE-pA (S0230-9-H50) were purchased from TaiTool. All virus were diluted with PBS to a final concentration of 5×10^{12} per mL before stereotaxic delivery into the mouse brain.

Body temperature recording

The rectal temperatures were recorded by animal temperature measuring apparatus (FT3400, Kew Basis) (Fig. 3C,3G and 3H; fig.S3C-E) every 30 minutes and the viscera temperature was recorded by IR digital thermographic camera (FLIR T430sc) every 5 minutes (Fig. 5F, 5G). The other internal temperatures were measured and recorded by Anilogger core temperature monitoring system every 15 minutes. The mice were adapted for 4 days before test. All temperature recording experiments were performed under ambient temperature at 24°C.

Middle cerebral artery occlusion (MCAO) and infarct volume evaluation

Adult male wistar rats were anesthetized with isoflurane. Rats were subjected to a right side MCAO[12,57] and heating lamps were utilized to maintain rectal temperature at 36.5 to 37.5°C. Reperfusion was achieved by the withdrawal of the filament after 2 h occlusion. In all ischemia models, solvent or P57 was immediately injected intraperitoneally once priming reperfusion.

Infarct volume was evaluated by TTC staining[12]. Briefly, rats were sacrificed at 24 h following reperfusion and their brain were quickly removed and chilled. Six coronal brain slices with a 2-mm thickness were cut for the treatment with 1% TTC solution at 37°C for 20 min, then fixed in 10% formalin solution. The images of the coronal slices were taken with a digital camera and analyzed to quantify the infarct area with Adobe Photoshop software. Infarct volumes were determined by the integration of the infarct area of each slice and the distances between them.

Affinity chromatography experiment and iTRAQ analysis

500 μL brain lysate was pre-incubated 1 hour with DMSO or 20 μM P57 at 4℃ with rotation, and then incubated 1 hour with DMSO or 2 μM P57-Bio at 4°C with rotation. The samples were added to 20 μL pre-washed high-capacity streptavidin agarose beads and incubated 1 hour at 4°C with rotation. The beads were pelleted and washed 4 times with lysis buffer. The wash buffer was aspirated completely from the beads. Then 50 μL 1× sample buffer was added and incubated for 5 min on a 95°C-heat block. The sample buffer containing proteins off the beads was carefully transferred to a new 1.5 mL Eppendorf tube, and was loaded onto 15% SDS-PAGE.

In-gel Digestion

After silver staining, the gel was washed with deionized water and gel lanes were excised using surgical scissors into pieces. Then gel pieces were reduced with 5 mM dithiothreitol (DTT) at 56°C for 1 h. Alkylation was followed by incubation with 15 mM iodoacetamide (IAA) in dark for 45min. After removed the supernatant, the samples were incubated with trypsin covering at 37°C for overnight. Transferred the supernatant into a clean tube. Squeezing the gels used 100% ACN (v/v) to ensure all the peptides could be extracted. Combined all the peptides and dried them by Speed-Vac. Then the peptides were dissolved in 0.1% TFA and further desalted with C18 Zip-tip.

LC–MS/MS Analysis

LC–MS/MS analysis was conducted using an EASY-nLC 1000 HPLC system (Thermo Fisher Scientific) and an Orbitrap Fusion (Thermo Fisher Scientific). The sample was reconstituted using buffer A (0.1% formic acid, 2% ACN) and then loaded onto C18 reversed phase capillary analytical column (3 μm particle size, 90 Å pore size) by the autosampler which connected to an EASY-nLC 1000 HPLC system. The peptides were eluted at constant flow rate of 300 nL/min by increasing buffer B (0.1% formic acid, 90% ACN) from 8–32% over 58 min, then 48% in 6 min followed a steep increase to 80% in 2 min.

The mass spectrometric analysis was carried out in a data dependent acquisition (DDA) mode with a cycle time of 3 s. The peptides with a range of m/z 350–1300 were detected by an Orbitrap mass analyzer. And the resolution was set as 120,000 at m/z 200. Automatic gain control (AGC) target and maximum ion injection time (IT) were 5.0 × 105 and 50 ms, respectively. The isolated precursor ions were subjected to fragmentation via higher-energy collisional dissociation (HCD) with a collision energy of 32%, and analyzed by ion trap analyzer. The dynamic exclusion was set as 60 s, and the charge inclusion state was set to 2 ~ 6+.

Data Analysis

The raw data were analyzed by Mascot search engine (v2.3.0) against the UniProt Mus musculus database (downloaded 2013). The parameters were set as following: Carbamidomethylation (C) and acetylation (protein N-terminal) were set as fixed modifications and oxidation (M) as variable modification. Trypsin was specific enzyme and allowed up to 2 missed cleavage. Mass tolerances were set to ± 10 ppm for precursor ions, ± 0.5 Da for fragment ions.

Western immunoblotting

Whole brain protein lysate was extracted using buffer containing 20 mM Tris-HCl (PH = 7.4), 100 mM KCl, 1% Triton-X-100 and complete protease inhibitors. The following antibodies were used for immunoblotting: PDXK (1:1000; 15309, Proteintech), GSTP1 (1:1000, 15902, Proteintech) and GAP43 (1:1000, 16971, Proteintech). Membranes were incubated overnight with primary antibody at 4°C, followed by 3X washes in PBST (PBS with 0.1% Triton-X-100, vol/vol) before incubation in secondary antibodies for 1 hour at room temperature. Images were captured using ChemiScope system (Clinx Science Instruments Co. Ltd).

Protein Expression and Purification

The coding sequences of wild-type full-length human PDXK and the site-directed mutant proteins (T47V, Y84E, D235A) were respectively subcloned into pET-28a vector resulting in the addition of an N-terminal His tag and thrombin cleavage site. The plasmids were transformed into Escherichia coli OverExpress C43(DE3) strain (2nd Lab, cat# EC1040) and induced with 0.4 mM IPTG at 18°C overnight. The fusion proteins were purified by HisTrap FF column (GE healthcare life sciences) after lysis of cells by sonication, followed by size-exclusion chromatography using a Superdex 75 column (GE healthcare life sciences). Once purified, the proteins were subsequently frozen in aliquots and stored in buffer (25 mM HEPES-NaOH, pH 7.5, 200 mM NaCl and 5% glycerol).

Microscale Thermophoresis (MST) Assay

A Monolith NT. Automated from NanoTemper Technologies was used for MST binding assay. Wild-type or mutant PDXK proteins were fluorescently labeled with the RED-tris-NTA (NanoTemper, cat# MO-L008) according to the manufacturer's instructions. All affinity measurements were performed in PBS buffer mixed with 0.05% Pluronic F-127 (Invitrogen, cat# P6866). Indicated compounds, arrayed at different concentrations, were incubated with proteins for 30 min before applied to Monolith NT standard treated

capillaries. Thermophoresis was then determined at 25°C with 15–20% excitation power and middle MST power. The data analysis was performed using the analysis software (MO. Affinity Analysis) after the measurement and plotted by GraphPad Prism 8.

Surface Plasmon Resonance (SPR) Assay

SPR experiments were performed on Biacore T200 instrument (GE healthcare). PDXK protein was covalently immobilized onto CM5 chip as standard procedure. The chip was equilibrated overnight first with HBS buffer (10 mM HEPES (PH = 7.4), 150 mM NaCl, 0.05% (v/v) surfactant P20 and 0.2% dimethyl sulfoxide). P57 was gradiently diluted with HBS buffer and then injected at 30 μL/min for 120 s contact time followed by dissociation for 300 s. Sensorgrams were fitted to the Langmuir binding equation for a 1:1 interaction model using Biacore T200 Evaluation Software v3.0 to determine kinetic parameters and equilibrium dissociation constants. Each experiment was performed at least three times.

Determination of Kinetic Constants

All PDXK kinetic measurements were carried out at 37℃ with 125 nM protein in 384-well plates (Corning, cat# 3702). Initial velocity studies for the conversion of PL to PLP were performed at 380 nm in an Agilant 8454 spectrophotometer (Thermo Fisher) in 100 mM sodium HEPES buffer, pH 7.4. The concentration of PL (J&K, cat# 322481) and Mg-ATP (Sigma, cat# A2383) were fixed at 2 mM and 1 mM respectively when titrating another substrate. Values for Km and K_{cat} were determined from Michaelis-Menten by GraphPad Prism 8.

Molecular Docking

Docking studies were performed with methods as previously published (https://doi.org/10.1016/j.ejmech.2019.111767) using Schrödinger suite (version 2009), which includes all of the programs described below. P57 was prepared through LigPrep panel integrated to generate all low-energy stereoisomers and possible ionization states in the pH range of 7.0 ± 2.0 with Epik. The crystal structure of PDXK in complex with PLP and ATP (PDB code 3KEU) was prepared using the Protein Preparation Wizard with default parameters. The ligand and protein were energy- minimized using OPLS-2005 force field. A PLP-centered receptor grid was generated with the program Glide. Then docking study was performed using Glide in extra-precision (XP) mode with enhanced planarity of conjugated pi groups, and strain correction terms applied.

Rotarod test

For the rotarod test, the mice were trained 2 days before test. On day 3, mice were placed on an accelerating rotarod cylinder, and the latency time of the animals was measured. The speed was increased from 5 to 40 rpm within 240 seconds. A trial ended if the animal fell off the rungs or gripped the device and spun around for 2 consecutive revolutions without attempting to walk on the rungs. Motor test data are presented as mean of latency time on the rotarod.

Open-field test

In the open-field test, each mouse was gently placed in the center of the box after intraperitoneal injection of P57, PL or solvent for 40 min respectively. Total distance travelled was recorded using the Ethovision XT video tracking software system (Noldus Information Technologies, Leesburg, VA, USA).

Metabolic Studies (CLAMS)

6 ~ 8-week-old C5BL/6J male mice were maintained individually in a metabolism chamber (Comprehensive Lab Animal Monitoring System, CLAMS) with free access to food and water for 72 hours. Mice were housed for 24 hours for adaption. On day 2, mice were intraperitoneally injected with solvent or P57 (12.5 mg/kg or 25 mg/kg). Metabolic parameters including O_2 consumption, CO_2 production, respiratory exchange ratio (RER), energy expenditure and total locomotor activity were recorded at 24 min intervals in a standard light-dark cycle (light 7:00–19:00 and dark 19:00–7:00) at 25°C. Respiratory quotient is the ratio of carbon dioxide production to oxygen consumption (VO_2). RER = VCO_2/VO_2. Energy expenditure was calculated as the product of the calorific value of oxygen ($3.815*VO_2 + 1.232*VCO_2$)[58].

Measurement of PL level in hypothalamus

Pyridoxine (PN), pyridoxamine (PM), pyridoxal (PL), 4-pyridoxic acid (4-PA), and pyridoxal 5'-phosphate (PLP) were analyzed on an Agilent 1260 Infinity liquid chromatography (Agilent, CA, USA) coupled with an AB SCIEX QTrap 6500 Mass Spectrometer (AB SCIEX, MA, USA) according to a method reported by Midttun et al. previously[59]. Pyridoxal-(methyl-d3) (PL-d3) was used as the internal standard to tract the extraction efficacy. The accuracy of each analyte was validated to be of more than 90% with the RSD of less than 10%.

Acute slice preparation and electrophysiology

Mouse brain slices were prepared according to previously published procedures [60]. Mouse was deeply anesthetized by isoflurane, and followed by transcardial perfusion with ice-cold, oxygenated (95% O_2 / 5% CO_2) artificial cerebrospinal fluid (ACSF) containing (in mM): 127 NaCl, 2.5 KCl, 25 $NaHCO_3$, 1.25 NaH_2PO_4, 2.0 $CaCl_2$, 1.0 $MgCl_2$, and 25 Glucose (osmolarity ~ 310 mOsm/L). After perfusion and decapitation, mouse brain was removed and immersed in ice-cold and oxygenated ACSF. Tissue was blocked and supported by a block of 4% agar, and transferred to a slicing chamber containing ice-cold and oxygenated ACSF. Coronal slices of 250-μm-thick were prepared on a vibratome (Series1000, Tissue Sectioning System, Natural Genetic Ltd., USA), in rostral/caudal direction. Slices were transferred to a chamber containing constantly oxygenated ACSF, and incubated at around 34 ˚C for 20 min before recording.

Brain slices were transferred to a recording chamber perfused with oxygenated ACSF at a flow rate of 1.5-2 ml/min, and temperature was maintained at ~ 30°C during recording by feedback in-line heater (TC-324C; Warner Instruments, Hamden, CT). MPA GABA and non-GABA neurons were visualized in slices using IR/DIC microscopy, and identified based on tdTomato signal in Vgat-ires-Cre; Ai14 mice. Cell-

attached recordings were established with glass pipettes (3–5 MΩ) containing the following (in mM): 135 K-gluconate, 4 KCl, 10 HEPES, 10 Na-phosphocreatine, 4 MgATP, 0.4 Na_2GTP, and 1 EGTA (with pH 7.2–7.3, and osmolarity ~ 295 mOsm/L). P57 (2 μM) or PL (10 μM) were applied by bath perfusion. Recordings were made using 700B amplifier and Digidata 1440A interface (Axon Instruments, Union City, CA). Signals were filtered at 4 kHz, sampled at 10 kHz, and analyzed using Clampex 10.7 (Molecular Devices).

Tissue processing, immunohistochemistry and imaging

Mice were deeply anesthetized with isoflurane, and perfused transcardially with 4% paraformaldehyde (PFA) in 0.1 M phosphate buffered saline (PBS). Brains were removed and post-fixed for 24 hours in 4% PFA at 4°C, followed by dehydrating with 20% and 30% sucrose for 24h in sequence. Dehydrated brains were embedded in OCT, and cut at 40 μm using a cryostat (CM1950, Leica). Tissues were chosen and pretreated in 0.2% Triton-X100 for an hour at room temperature (RT), then blocked with 0.05% Triton-X100, 10% bovine serum albumin (BSA) in PBS for one hour at RT and rinsed in PBS. Tissues were transferred into primary antibody solution (Rabbit anti-cFos, 1:1000, Cell Signaling) in PBS with 0.2% Triton-X100 and incubated for 24 hours at 4°C. Tissues were rinsed in PBS for three times, and incubated with secondary antibody solution (Goat anti-Rabbit 647, 1:800, Life Technologies) in PBS for 2 hours at RT, then rinsed with PBS for three times and mounted onto slides, dried and covered under glycerol: TBS (3:1) with Hoechst 33342 (1:1000, ThermoFisher Scientific). Sections were imaged with an Olympus VS120 slide scanning microscope. Confocal images were acquired with a Nikon A1 confocal laser scanning microscope with an X25 objective. Images were analyzed in ImageJ (FIJI).

In vivo **fiber photometry calcium signal recording**

For *in vivo* fiber photometry recording, AAV-hSyn-DIO-jGCaMP7s viruses were injected into MPA of Vgat-ires-Cre and Vglut2-ires-Cre mice with a microsyringe pump controller (NanoJect III, Drummond Scientific Company). Three weeks after virus injection, an optical fiber (400 μm, 0.57 NA, MFC_400/430, Doric Lens) was implanted into MPA. During optical fiber implantation, we monitored the change of fluorescence intensity in real-time with photometry recording system (Doric Lens). GCamp7s was excited with sinusoidally modulated light from laser diode modules at 465 nm (211 Hz) and 405 nm (531 Hz). Signals emitted from GCamp7s and its isosbestic control channel were acquired using a photoreceiver (H10722-20; Hamamatsu Photonics), digitized at 500 Hz, and then recorded by Doric Neuroscience Studio Software. The final depth of implantation was determined by the cessation of further increases of fluorescence intensity, and optical fiber was secured with dental cement. Mice were housed for at least 1 week for recovery before recording. During recording, mouse was placed in its home cage with an optical fiber patch cord connected to the implanted optical fiber. Changes in fluorescence with time were calculated by smoothing signals from the isosbestic control channel. Relative fluorescence intensity was defined as the signal intensity change relative to the first 5-min baseline recording before i.p. injection. Mouse core body temperature was monitored every 5 min with a thermal camera (FLIR T430sc) during recording.

Hypothalamic snRNA-seq

Raw data quality (Fastq format) was assessed and poor-quality reads were removed using fastp (version 0.19.5) program[61] with the following parameters: “-n 15 –q 20 –u 50 –w 16”. Cleaned data were then mapped to reference genome (mm10) using the default parameters of Cell Ranger v6.0.2 (10X Genomics). Since both un-spliced pre-mRNA and mature mRNA were captured in snRNA-seq strategy, we set the parameter “–include-introns” in Cell Ranger pipeline, which enables us to counts these unspliced reads.

Seurat (version 4.0)[62] was used to process and cluster cells. For this analysis, three S4 objects, one for each group (P57, PL, and control) were created using the *Read10X* and *CreateSeuratObject* functions with the parameter *min.cell = 3* to filter genes expressed in fewer than 3 cells. The percent of ribosomal protein transcripts (percent.RP), the percent of mitochondrial transcripts (percent.MT), the number of genes detected per cell (nFeature_RNA) and the percent of erythrocyte transcripts (percent.HB) were used to assess cell quality. We removed the low-quality cells by setting cut-off: 200 < nFeature_RNA < 6000, percent.MT < 10, percent.HB < 5, percent.RP < 3. To eliminate the effects of different sequencing depth, we normalized the data using *NormalizeData* function with the following parameters: normalization.method = "LogNormalize", scale.factor = 10000. Then, using the “vst” method to find 2000 high variable genes (HVGs) by *FindVariableFeatures* function, these HVGs would be the features in the principal component analysis (PCA). Before PCA analysis (*RunPCA* function), the data was scaled using the *ScaleData* function. Clustering was done by using the *FindNeighbors* function, using the top 15 principal components (PCs) and the *FindClusters* function.

Cell type annotation was performed with *SingleR* (version 1.6.1)[63]. If a cluster co-expresses markers of two cell types, then the cluster likely contains double-droplets. Based on this, we excluded total 965 cells using the default parameters of the R package *DoubletFinder* (version 2.0) from three groups (P57, PL, and control)[64]. For visualization and analysis and to eliminate batch effects, the three groups were integrated as a Seurat object using Harmony (version 0.1.0)[65]. Then, the integrated object was clustered using FindClusters function with the *resolution = 0.4*. In addition, Glutamatergic neurons and GABAergic neurons were extracted and clustered to 39 subpopulations by setting the *resolution = 1.5*. We performed *FindAllMarkers* function to identify the marker gene of each cluster by setting cut-off: *min.pct = 0.1, logfc.threshold = 0.25, test.use = "wilcox"*. The DEGs between different groups was calculated by using FindMarker function, such as P57_vs_Control: *FindMarkers (object, ident.1 = “P57”, ident.2 = "control")*.

To explore the potential function of marker genes in different cell populations or DEGs in different groups, we used R package *clusterProfiler (version 4.0.5)* to perform KEGG Function enrichment analysis. The *org.Mm.eg.db* package was used to set the background gene list as all genes detected in sequencing. The Benjamin-Hochberg FDR method was used to adjust the right tail P-value (two-sided binomial statistical test).

Declarations

Acknowledgements

We thank instructive advice and support from prof. Lan Ma and Feifei Wang from Fudan University and prof. Jun O. Liu from Johns Hopkins University. This work was supported by the National Natural Science Foundation of China [22137002, 21877016 to Y.D.; 22031011, 21621002 to B.Y.; 91853205, 81625022 to C.L.; 81972621 to W.J. and 81970727, 31900738 to L.X.], the Fund of the State Key Laboratory of Bioorganic and Natural Products Chemistry [SKLBNPC16233], the Key Research Program of Frontier Sciences of the Chinese Academy of Sciences [ZDBS-LY-SLH030], Shanghai Municipal Science and Technology Major Project (No.2018SHZDZX01), Shanghai Pujiang Program (19PJ1401800), ZJLab, and Shanghai Center for Brain Science and Brain-Inspired Technology.

Author contributions

Y.D. initiates the project, Y.D., B.Y., C.L. and W.J. designed and supervised the project; R.W. and L.X. did experiments and analyzed and prepared data; J.P. and Q.M. did single cell experiments and analyzed the data; D.Z. and R.W. contributed to molecular biological and animal experiments; C.P. and W.L. contributed to chemical synthesis; J.W. and J.H. contributed to enzyme activity assay and computational calculation; M.Z. and M.T. contributed to identification of target protein by MS; G.W., L.G., Q.T., M.J., M.H., Y.W., Z.L. and C.L. contributed to neurobiological experiments; T.L. contributed to MACO model; J.L. contributed to HPLC experiments; the manuscript was written by R.W., L.X., W.J. and Y.D.

Competing interests

The authors declare no competing interests.

Data and materials availability: All data in this paper are presented in the main text and supplementary materials.

References

1. Stephen A Bernard 1, T. W. G., Michael D Buist, Bruce M Jones, William Silvester, Geoff Gutteridge, Karen Smith. Treatment of comatose survivors of out-of-hospital cardiac arrest with induced hypothermia. N Engl J Med **346**, 557–563 (2002).
2. Mild therapeutic hypothermia to improve the neurologic outcome after cardiac arrest. N Engl J Med **346**, 549–556 (2002).
3. Scirica, B. M. Therapeutic hypothermia after cardiac arrest. Circulation **127**, 244–250, doi:10.1161/CIRCULATIONAHA.111.076851 (2013).
4. Kohlhauer, M. *et al.* Protection against cardiac ischemia-reperfusion injury by hypothermia and by inhibition of succinate accumulation and oxidation is additive. Basic Res Cardiol **114**, 18, doi:10.1007/s00395-019-0727-0 (2019).

5. Gluckman, P. D. *et al.* Selective head cooling with mild systemic hypothermia after neonatal encephalopathy: multicentre randomised trial. The Lancet **365**, 663–670, doi:10.1016/s0140-6736(05)17946-x (2005).
6. Jacobs, S. E. *et al.* Whole-body hypothermia for term and near-term newborns with hypoxic-ischemic encephalopathy: a randomized controlled trial. Arch Pediatr Adolesc Med **165**, 692–700, doi:10.1001/archpediatrics.2011.43 (2011).
7. Polderman, K. H., Tjong Tjin Joe, R., Peerdeman, S. M., Vandertop, W. P. & Girbes, A. R. Effects of therapeutic hypothermia on intracranial pressure and outcome in patients with severe head injury. Intensive Care Med **28**, 1563–1573, doi:10.1007/s00134-002-1511-3 (2002).
8. Zhi, D., Zhang, S. & Lin, X. Study on therapeutic mechanism and clinical effect of mild hypothermia in patients with severe head injury. Surgical Neurology **59**, 381–385, doi:10.1016/s0090-3019(03)00148-4 (2003).
9. Rawls, S. M. CB1 Receptors in the Preoptic Anterior Hypothalamus Regulate WIN 55212-2 [(4,5-Dihydro-2-methyl-4(4-morpholinylmethyl)-1-(1-naphthalenyl-carbonyl)-6H-pyrrolo[3,2,1ij]quinolin-6-one]-Induced Hypothermia. Journal of Pharmacology and Experimental Therapeutics **301**(**3**), 963–968 (2002).
10. Bonfils, P. K., Reith, J., Hasseldam, H. & Johansen, F. F. Estimation of the hypothermic component in neuroprotection provided by cannabinoids following cerebral ischemia. Neurochem Int **49**, 508–518, doi:10.1016/j.neuint.2006.03.015 (2006).
11. Leker, R. R., Gai, N., Mechoulam, R. & Ovadia, H. Drug-induced hypothermia reduces ischemic damage: effects of the cannabinoid HU-210. Stroke **34**, 2000–2006, doi:10.1161/01.STR.0000079817.68944.1E (2003).
12. Suzuki, N. *et al.* Contribution of hypothermia and CB1 receptor activation to protective effects of TAK-937, a cannabinoid receptor agonist, in rat transient MCAO model. PLoS One **7**, e40889, doi:10.1371/journal.pone.0040889 (2012).
13. Zhijuan Cao, A. B., 2and Sean P. Marrelli,. Pharmacologically induced hypothermia via TRPV1 channel agonism provides neuroprotection following ischemic stroke when initiated 90 min after reperfusion. Am J Physiol Regul Integr Comp Physiol **306**, R149–R156, doi:10.1152/ajpregu.00329.2013.-Traditional (2014).
14. Muzzi, M. *et al.* Ischemic Neuroprotection by TRPV1 Receptor-Induced Hypothermia. Journal of Cerebral Blood Flow & Metabolism **32**, 978–982, doi:10.1038/jcbfm.2012.36 (2012).
15. Baker, A. K. & Meert, T. F. Functional effects of systemically administered agonists and antagonists of mu, delta, and kappa opioid receptor subtypes on body temperature in mice. The Journal of pharmacology and experimental therapeutics **302**, 1253–1264, doi:10.1124/jpet.102.037655 (2002).
16. Rawls, S. M. Effects of opioids cannabinoids and vanilloids on body temperature. Frontiers in Bioscience, **S3**(**3**), 822–845 (2011).
17. Benamar, K., Geller, E. B. & Adler, M. W. Role of the nitric oxide pathway in kappa-opioid-induced hypothermia in rats. The Journal of pharmacology and experimental therapeutics **303**, 375–378,

doi:10.1124/jpet.102.036269 (2002).

18. Zhang, Z. *et al.* Kappa-opioid receptor selectivity for ischemic neuroprotection with BRL 52537 in rats. Anesthesia and analgesia **97**, 1776–1783, doi:10.1213/01.ane.0000087800.56290.2e (2003).
19. Sigg, D. C., Coles, J. A., Jr., Oeltgen, P. R. & Iaizzo, P. A. Role of delta-opioid receptor agonists on infarct size reduction in swine. American journal of physiology. Heart and circulatory physiology **282**, H1953-1960, doi:10.1152/ajpheart.01045.2001 (2002).
20. Drabek, T. *et al.* Assessment of the delta opioid agonist DADLE in a rat model of lethal hemorrhage treated by emergency preservation and resuscitation. Resuscitation **77**, 220–228, doi:10.1016/j.resuscitation.2007.11.020 (2008).
21. Bissette, G., Nemeroff, C. B., Loosen, P. T., Prange, A. J., Jr. & Lipton, M. A. Hypothermia and intolerance to cold induced by intracisternal administration of the hypothalamic peptide neurotensin. Nature **262**, 607–609, doi:10.1038/262607a0 (1976).
22. Katz, L. M., Wang, Y., McMahon, B. & Richelson, E. Neurotensin analog NT69L induces rapid and prolonged hypothermia after hypoxic ischemia. Acad Emerg Med **8**, 1115–1121, doi:10.1111/j.1553-2712.2001.tb01126.x (2001).
23. Torup, L., Borsdal, J. & Sager, T. Neuroprotective effect of the neurotensin analogue JMV-449 in a mouse model of permanent middle cerebral ischaemia. Neurosci Lett **351**, 173–176, doi:10.1016/j.neulet.2003.08.008 (2003).
24. Wei, S. *et al.* Acute and delayed protective effects of pharmacologically induced hypothermia in an intracerebral hemorrhage stroke model of mice. Neuroscience **252**, 489–500, doi:10.1016/j.neuroscience.2013.07.052 (2013).
25. Gu, X. *et al.* Pharmacologically induced hypothermia attenuates traumatic brain injury in neonatal rats. Exp Neurol **267**, 135–142, doi:10.1016/j.expneurol.2015.02.029 (2015).
26. Doyle, K. P. *et al.* Novel thyroxine derivatives, thyronamine and 3-iodothyronamine, induce transient hypothermia and marked neuroprotection against stroke injury. Stroke **38**, 2569–2576, doi:10.1161/STROKEAHA.106.480277 (2007).
27. Panas, H. N. *et al.* Normal thermoregulatory responses to 3-iodothyronamine, trace amines and amphetamine-like psychostimulants in trace amine associated receptor 1 knockout mice. Journal of neuroscience research **88**, 1962–1969, doi:10.1002/jnr.22367 (2010).
28. Tan, C. L. & Knight, Z. A. Regulation of Body Temperature by the Nervous System. Neuron **98**, 31–48, doi:10.1016/j.neuron.2018.02.022 (2018).
29. Zhao, Z. D. *et al.* A hypothalamic circuit that controls body temperature. Proc Natl Acad Sci U S A **114**, 2042–2047, doi:10.1073/pnas.1616255114 (2017).
30. Van Heerden, F. R. Hoodia gordonii: A natural appetite suppressant. Journal of Ethnopharmacology **119**, 434–437, doi:10.1016/j.jep.2008.08.023 (2008).
31. van Heerden, F. R. *et al.* An appetite suppressant from Hoodia species. Phytochemistry **68**, 2545–2553, doi:10.1016/j.phytochem.2007.05.022 (2007).

32. Geiser, F. Hibernation. Curr Biol **23**, R188-193, doi:10.1016/j.cub.2013.01.062 (2013).
33. Talma, N. *et al.* Neuroprotective hypothermia - Why keep your head cool during ischemia and reperfusion. Biochim Biophys Acta **1860**, 2521–2528, doi:10.1016/j.bbagen.2016.07.024 (2016).
34. Kuczynski, A. M., Demchuk, A. M. & Almekhlafi, M. A. Therapeutic hypothermia: Applications in adults with acute ischemic stroke. Brain Circ **5**, 43–54, doi:10.4103/bc.bc_5_19 (2019).
35. Kurisu, K. & Yenari, M. A. Therapeutic hypothermia for ischemic stroke; pathophysiology and future promise. Neuropharmacology **134**, 302–309, doi:10.1016/j.neuropharm.2017.08.025 (2018).
36. Forreider, B., Pozivilko, D., Kawaji, Q., Geng, X. & Ding, Y. Hibernation-like neuroprotection in stroke by attenuating brain metabolic dysfunction. Prog Neurobiol **157**, 174–187, doi:10.1016/j.pneurobio.2016.03.002 (2017).
37. Madgula, V. L. *et al.* Bioavailability, pharmacokinetics, and tissue distribution of the oxypregnane steroidal glycoside P57AS3 (P57) from Hoodia gordonii in mouse model. Planta medica **76**, 1582–1586, doi:10.1055/s-0030-1249818 (2010).
38. Cui, Z. *et al.* Ethacrynic acid targets GSTM1 to ameliorate obesity by promoting browning of white adipocytes. Protein Cell, doi:10.1007/s13238-020-00717-7 (2020).
39. Gandhi, A. K. *et al.* Kinetic and structural studies of the role of the active site residue Asp235 of human pyridoxal kinase. Biochem Biophys Res Commun **381**, 12–15, doi:10.1016/j.bbrc.2009.01.170 (2009).
40. Boulant, J. A. Hypothalamic mechanisms in thermoregulation. Fed Proc **40**, 2843–2850 (1981).
41. Nakayama, T. Thermosensitive neurons in the brain. Jpn J Physiol **35**, 375–389, doi:10.2170/jjphysiol.35.375 (1985).
42. Rouillard, A. D. *et al.* The harmonizome: a collection of processed datasets gathered to serve and mine knowledge about genes and proteins. *Database (Oxford)* 2016, doi:10.1093/database/baw100 (2016).
43. Zhang, Z. *et al.* Estrogen-sensitive medial preoptic area neurons coordinate torpor in mice. Nature communications **11**, 6378, doi:10.1038/s41467-020-20050-1 (2020).
44. Hrvatin, S. *et al.* Neurons that regulate mouse torpor. Nature **583**, 115–121, doi:10.1038/s41586-020-2387-5 (2020).
45. Takahashi, T. M. *et al.* A discrete neuronal circuit induces a hibernation-like state in rodents. Nature, doi:10.1038/s41586-020-2163-6 (2020).
46. MacLean, D. B. & Luo, L. G. Increased ATP content/production in the hypothalamus may be a signal for energy-sensing of satiety: studies of the anorectic mechanism of a plant steroidal glycoside. Brain research **1020**, 1–11, doi:10.1016/j.brainres.2004.04.041 (2004).
47. Boris Le Nevé, M. F., 2 Hannelore Daniel,1 and Robin Gouka2. The steroid glycoside H.g.-12 from Hoodia gordonii activates the human bitter receptor TAS2R14 and induces CCK release from HuTu-80 cells. *Am J Physiol Gastrointest Liver Physiol* **299**, G1368–G1375, doi:10.1152/ajpgi.00135.2010.-Steroid (2010).

48. Wilson, M. P., Plecko, B., Mills, P. B. & Clayton, P. T. Disorders affecting vitamin B6 metabolism. J Inherit Metab Dis, doi:10.1002/jimd.12060 (2019).
49. Chelban, V. *et al.* PDXK mutations cause polyneuropathy responsive to pyridoxal 5'-phosphate supplementation. Ann Neurol **86**, 225–240, doi:10.1002/ana.25524 (2019).
50. Yu, S. *et al.* Glutamatergic Preoptic Area Neurons That Express Leptin Receptors Drive Temperature-Dependent Body Weight Homeostasis. The Journal of neuroscience: the official journal of the Society for Neuroscience **36**, 5034–5046, doi:10.1523/JNEUROSCI.0213-16.2016 (2016).
51. Song, K. *et al.* The TRPM2 channel is a hypothalamic heat sensor that limits fever and can drive hypothermia. Science **353**, 1393–1398 (2016).
52. Tan, C. L. *et al.* Warm-Sensitive Neurons that Control Body Temperature. *Cell* **167**, 47–59 e15, doi:10.1016/j.cell.2016.08.028 (2016).
53. Cakir, I. *et al.* Leptin Receptor Signaling in Sim1-Expressing Neurons Regulates Body Temperature and Adaptive Thermogenesis. Endocrinology **160**, 863–879, doi:10.1210/en.2019-00062 (2019).
54. Akira Takahashi, H. I., Yasushi Ikarashi, Eiko Kishi, Yuji Maruyama. Opposite regulation of body temperature by cholinergic input to the paraventricular nucleus and supraoptic nucleus in rats. Brain research **99**, 102–111 (2001).
55. Wang, P. *et al.* A leptin-BDNF pathway regulating sympathetic innervation of adipose tissue. Nature, doi:10.1038/s41586-020-2527-y (2020).
56. Zhang, J., Shi, H., Ma, Y. & Yu, B. Expeditious synthesis of saponin P57, an appetite suppressant from Hoodia plants. Chemical communications (Cambridge, England) **48**, 8679–8681, doi:10.1039/c2cc34404a (2012).
57. Geng, X. *et al.* Neuroprotection by Chlorpromazine and Promethazine in Severe Transient and Permanent Ischemic Stroke. Molecular neurobiology **54**, 8140–8150, doi:10.1007/s12035-016-0280-x (2017).
58. Lee, J. *et al.* Withaferin A is a leptin sensitizer with strong antidiabetic properties in mice. Nature medicine **22**, 1023–1032, doi:10.1038/nm.4145 (2016).
59. Midttun, O., Hustad, S. & Ueland, P. M. Quantitative profiling of biomarkers related to B-vitamin status, tryptophan metabolism and inflammation in human plasma by liquid chromatography/tandem mass spectrometry. Rapid Commun Mass Spectrom **23**, 1371–1379, doi:10.1002/rcm.4013 (2009).
60. Xiao, L., Priest, M. F., Nasenbeny, J., Lu, T. & Kozorovitskiy, Y. Biased Oxytocinergic Modulation of Midbrain Dopamine Systems. *Neuron* **95**, 368–384 e365, doi:10.1016/j.neuron.2017.06.003 (2017).
61. Chen, S., Zhou, Y., Chen, Y. & Gu, J. fastp: an ultra-fast all-in-one FASTQ preprocessor. Bioinformatics **34**, i884-i890, doi:10.1093/bioinformatics/bty560 (2018).
62. Hao, Y. *et al.* Integrated analysis of multimodal single-cell data. *Cell* **184**, 3573–3587 e3529, doi:10.1016/j.cell.2021.04.048 (2021).
63. Aran, D. *et al.* Reference-based analysis of lung single-cell sequencing reveals a transitional profibrotic macrophage. Nat Immunol **20**, 163–172, doi:10.1038/s41590-018-0276-y (2019).

64. McGinnis, C. S., Murrow, L. M. & Gartner, Z. J. DoubletFinder: Doublet Detection in Single-Cell RNA Sequencing Data Using Artificial Nearest Neighbors. Cell Syst **8**, 329–337 e324, doi:10.1016/j.cels.2019.03.003 (2019).
65. Tran, H. T. N. *et al.* A benchmark of batch-effect correction methods for single-cell RNA sequencing data. Genome Biol **21**, 12, doi:10.1186/s13059-019-1850-9 (2020).

Figures

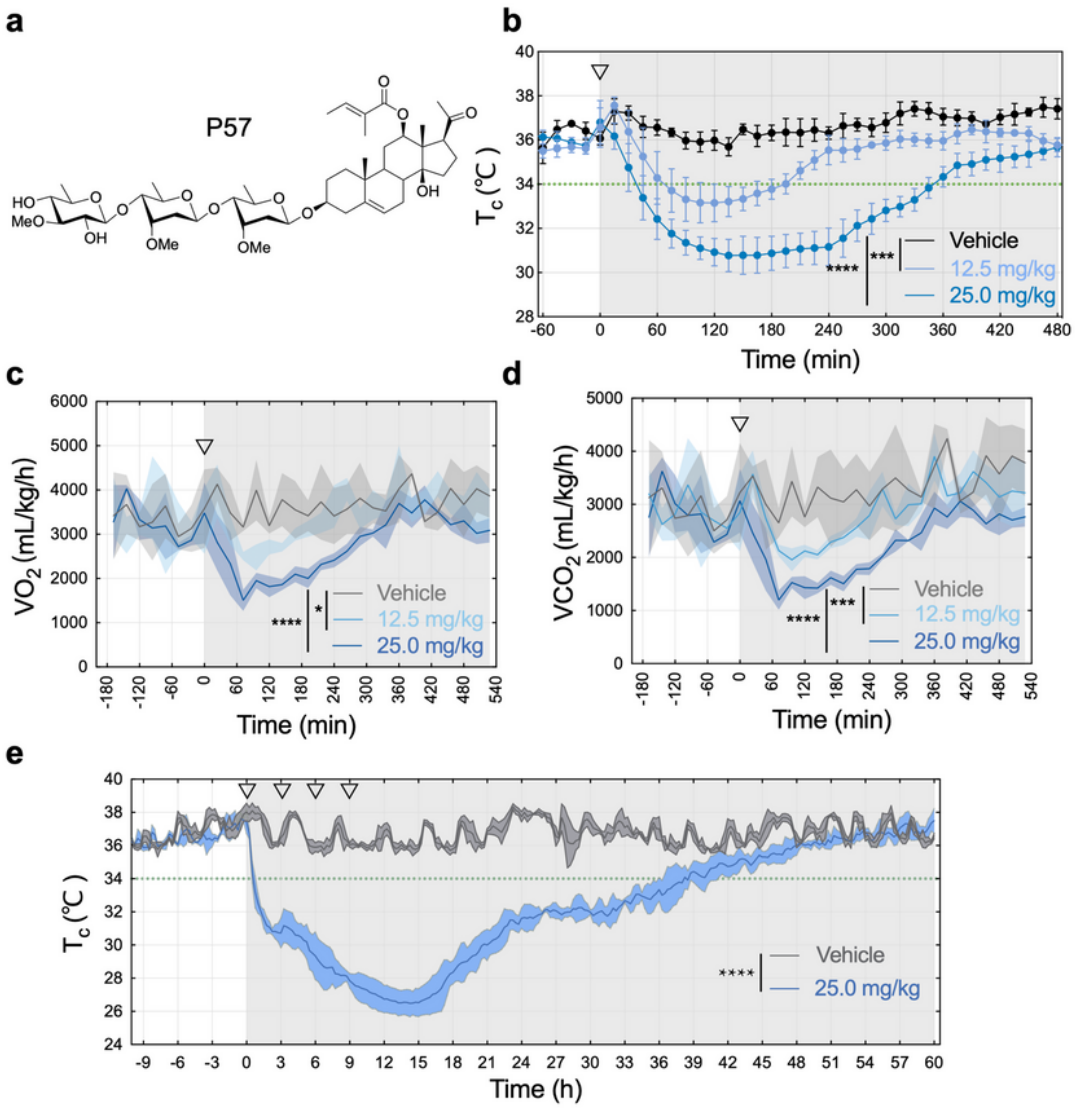

Figure 1

Figure 1

P57 induces a hibernation-like/torpor state in rodents. a, Chemical structure of P57. **b,** Core temperature of P57-treated mice. P57 (12.5 mg/kg or 25.0 mg/kg) or the vehicle control was injected intraperitoneally into mice at 0 min (arrow). Core temperature (T_C) was measured and recorded by Anilogger^R core temperature monitoring system every 15 minutes, mean (n = 5) ± s.d.; significant differences between treatments were calculated using two-way analysis of variance (ANOVA), *** P < 0.001 and **** P <

0.0001. **c,** Oxygen consumption level of P57-treated mice. P57 (12.5 mg/kg or 25.0 mg/kg) or the vehicle control was injected intraperitoneally into mice at 0 min (arrow). Volume of oxygen (VO_2) was measured every 24 minutes, mean (n = 3) ± s.d.; significant differences between treatments were calculated using two-way analysis of variance (ANOVA), * P < 0.05 and **** P < 0.0001. **d,** Carbon dioxide output level of P57-treated mice. P57 (12.5 mg/kg or 25.0 mg/kg) or the vehicle control was injected intraperitoneally into mice at 0 min (arrow). Volume of Carbon dioxide (VCO_2) was measured every 24 minutes, mean (n = 3) ± s.d.; significant differences between treatments were calculated using two-way analysis of variance (ANOVA), *** P < 0.001 and **** P < 0.0001. **e,** Core temperature of mice treated with P57 for four times. P57 (25.0 mg/kg) or the vehicle control was injected intraperitoneally into mice at 0, 3, 6 and 9 hours (arrow). Core temperature (T_C) was measured and recorded by Anilogger^R core temperature monitoring system every 15 minutes, mean (n = 3) ± s.d.; significant differences between treatments were calculated using two-way analysis of variance (ANOVA), **** P < 0.0001.

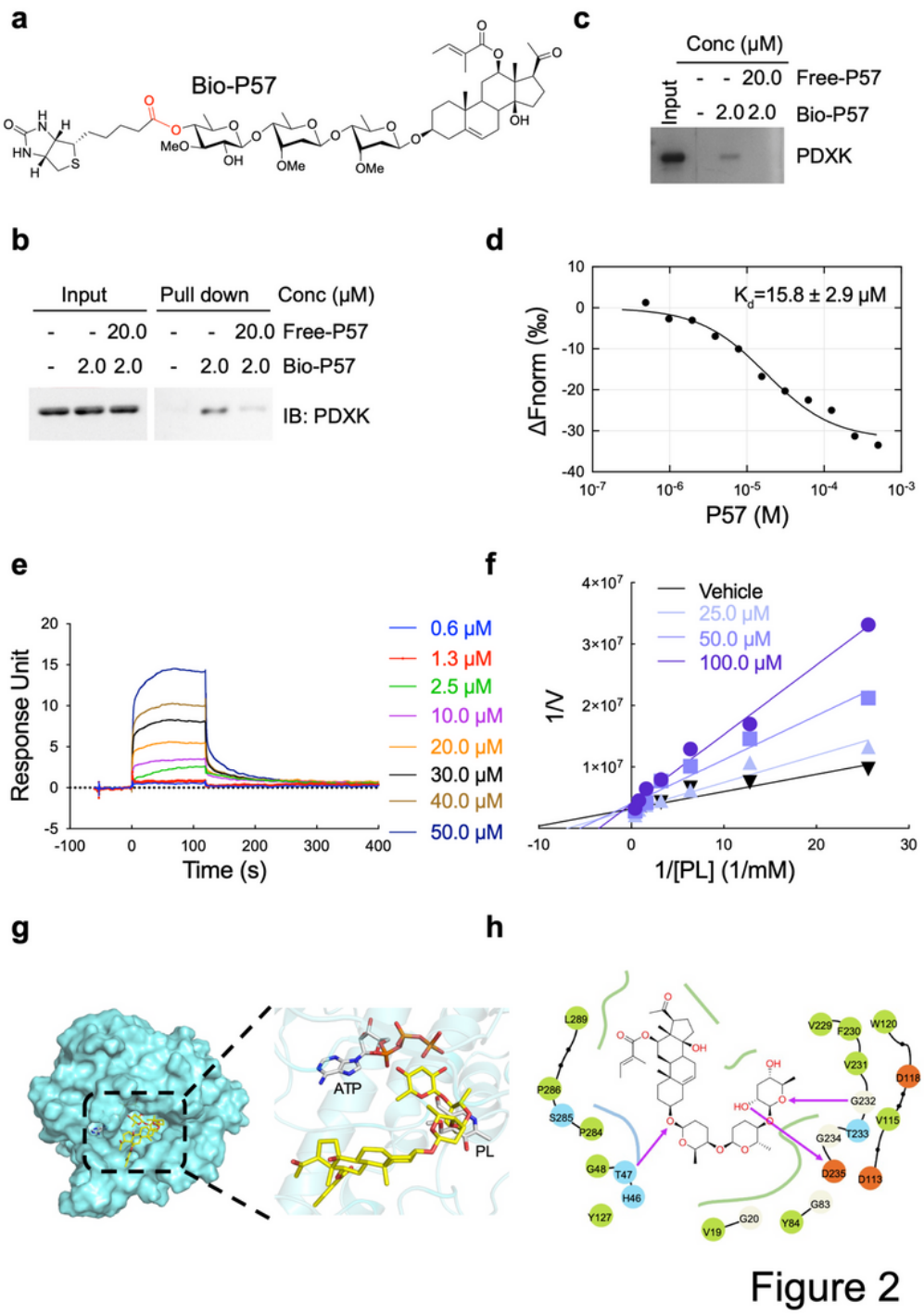

Figure 2

Figure 2

P57 binds with PDXK and inhibits its enzyme activity. a, Chemical structure of biotinylated P57 probe. **b, c,** Affinity chromatography experiment with mouse brain lysate (**b**) or purified protein PDXK (**c**) using P57-Bio (2.0 μM) probe in the absence (middle lane) and presence (right lane) of P57 (20.0 μM). **b,** Western blot was performed to measure the binding amount of PDXK with P57-Bio. **c,** Silver staining was performed to measure the binding amount of PDXK with P57-Bio. **d,** Dose-response curve for the binding

interaction between P57 and PDXK using MST. The concentration of purified protein PDXK is kept constant, while the concentration of P57 varies from 0 to 100 μM. The binding curve yields a dissociation constant K_d = 15.8 ± 2.9 μM. **e,** A surface plasmon resonance (SPR) assay characterizing the binding between P57 and purified protein PDXK. Color lines, model fits of SPR data from different concentrations of P57. The calculated dissociation constant K_d = 3.5 μM. **f,** Kinetic analysis of PDXK inhibition by P57 with respect to the substrate pyridoxal (PL) shows that P57 acts as a competitive inhibitor. **g,** A surface rendering of predicted binding mode of P57 (stick rendering) at the active site of human PDXK (cyan). Interactions between P57 and surrounding residues of PDXK, critical residues are rendered in stick representation (C, cyan; N, blue; O, red; H, grey), hydrogen-bond interactions are shown as black dashed lines. **h,** 2D-dimensional interaction schemes of predicted binding pose of P57 in ATP/PL active site generated by Maestro[39]. Magenta lines with arrow denote hydrogen bonds.

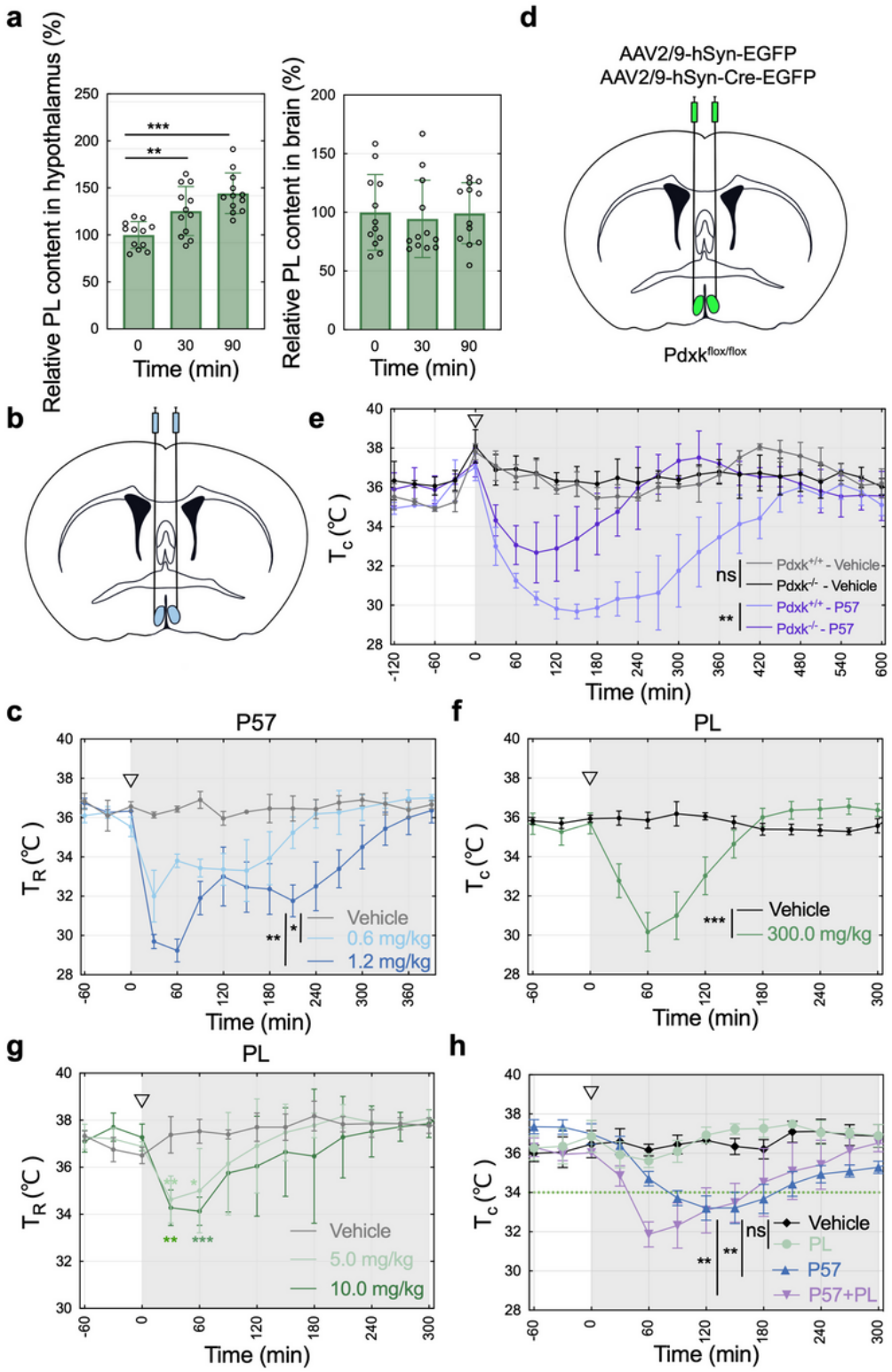

Figure 3

P57 mainly targets PDXK in hypothalamus to induces hypothermia. a, LC-MS detection of PL in hypothalamus (left) and brain tissues (right). Hypothalamus and brain tissue were sampled at 0 min, 30 min and 90 min after treated with P57 (25.0 mg/kg), mean (n = 12) ± s.d.; ** P < 0.01 and *** P < 0.001 compared to control group, as determined by student's t test. Detection of PL in tissues was confirmed by mass and retention time relative to the pure standard. **b,** Schematic showing the bilateral injection of P57

or PL into the POA. POA, preoptic area. **c,** Core temperature of mice treated with P57 in the POA. P57 (0.6 mg/kg or 1.2 mg/kg) or the vehicle control was injected into the POA at 0 min (arrow). Rectal temperature (T_R) was measured every 30 minutes, mean (n = 3) ± s.d.; significant differences between treatments were calculated using two-way analysis of variance (ANOVA), * P < 0.05 and ** P < 0.01. **d,** Schematic showing the bilateral injection of AAV2/9-hSyn-EGFP-WPRE-pA or AAV2/9-hSyn-Cre-EGFP-WPRE-pA into the MPA. **e,** Core temperature of P57-treated mice followed by knockout the PDXK in MPA. AAV-2/9-hSyn-EGFP-WPRE-pA or AAV2/9-hSyn-Cre-EGFP-WPRE-pA was injected into hypothalamus bilaterally for one month, then P57 (25 mg/kg) or the vehicle was injected intraperitoneally into mice at 0 min (arrow). Core temperature (T_C) was measured and recorded by Anilogger^R core temperature monitoring system every 30 minutes, mean (n = 3) ± s.d.; significant differences between treatments were calculated using two-way analysis of variance (ANOVA), ** P < 0.01. **f,** Core temperature of PL-treated mice. PL (300.0 mg/kg) or the vehicle was injected intraperitoneally into mice at 0 min (arrow). Core temperature (T_C) was measured and recorded by Anilogger^R core temperature monitoring system every 30 minutes, mean (n = 6) ± s.d.; significant differences between treatments were calculated using two-way analysis of variance (ANOVA), *** P < 0.001. **g,** Core temperature of mice treated with PL in the POA. PL (5.0 mg/kg or 10.0 mg/kg) or the vehicle was injected directly into the POA of C57BL/6J male mice at 0 min (arrow), mean (n = 4) ± s.d. * P < 0.05, ** P < 0.01 and *** P < 0.001 compared to control group, as determined by student's t test. **h,** Core temperature of mice treated with combination of PL (200.0 mg/kg) and P57 (12.5 mg/kg). PL (200.0 mg/kg) or P57 (12.5 mg/kg) was injected intraperitoneally into C57BL/6J male mice at 0 min (arrow). Core temperature (T_C) was measured and recorded by Anilogger^R core temperature monitoring system every 30 minutes, mean (n = 5) ± s.d.; significant differences between treatments were calculated using two-way analysis of variance (ANOVA); Ns, not significant; ** P < 0.01.

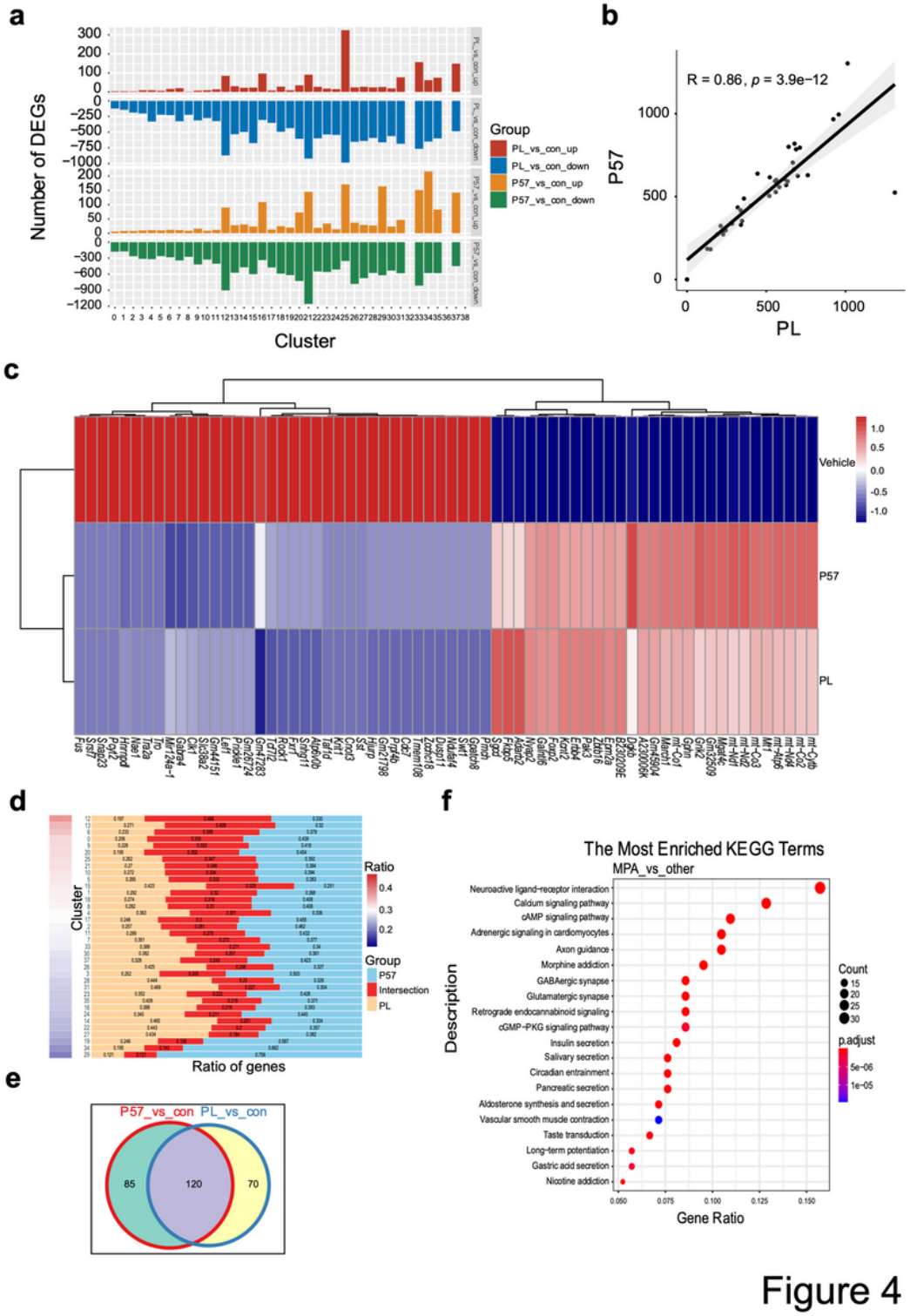

Figure 4

Figure 4

P57 and PL play a similar effect on hypothalamus neurons. a, Bar plot showing the number of DEGs affected by P57 and PL across each cluster in hypothalamic neuron subtypes. **b,** Scatter plot shows the correlation of the number of DEGs affected by P57 and PL. Each point represents a cluster, the value means the number of DEGs in each cluster. The linear best fit line is shown, and the Pearson correlation coefficient (R) and p-value (P) were calculated. **c,** Heatmap of shared DEGs in hypothalamus with P57

and PL treatment. **d,** The relative ratio of unique and overlapped DEGs between P57 and PL pair in each cluster. The burlywood and skyblue represents the number of specific DEGs of PL and P57 respectively, and the red stands for the number of overlapped DEGs. The heatmap on the left ranks each cluster by the Jaccard Similarity in DEGs between P57/PL and control group. **e,** Venn plot shows the overlap of DEGs of P57 and PL in the MPA compared with control group, respectively. **f,** KEGG pathway enrichment analysis of DEGs in the MPA and all other neurons.

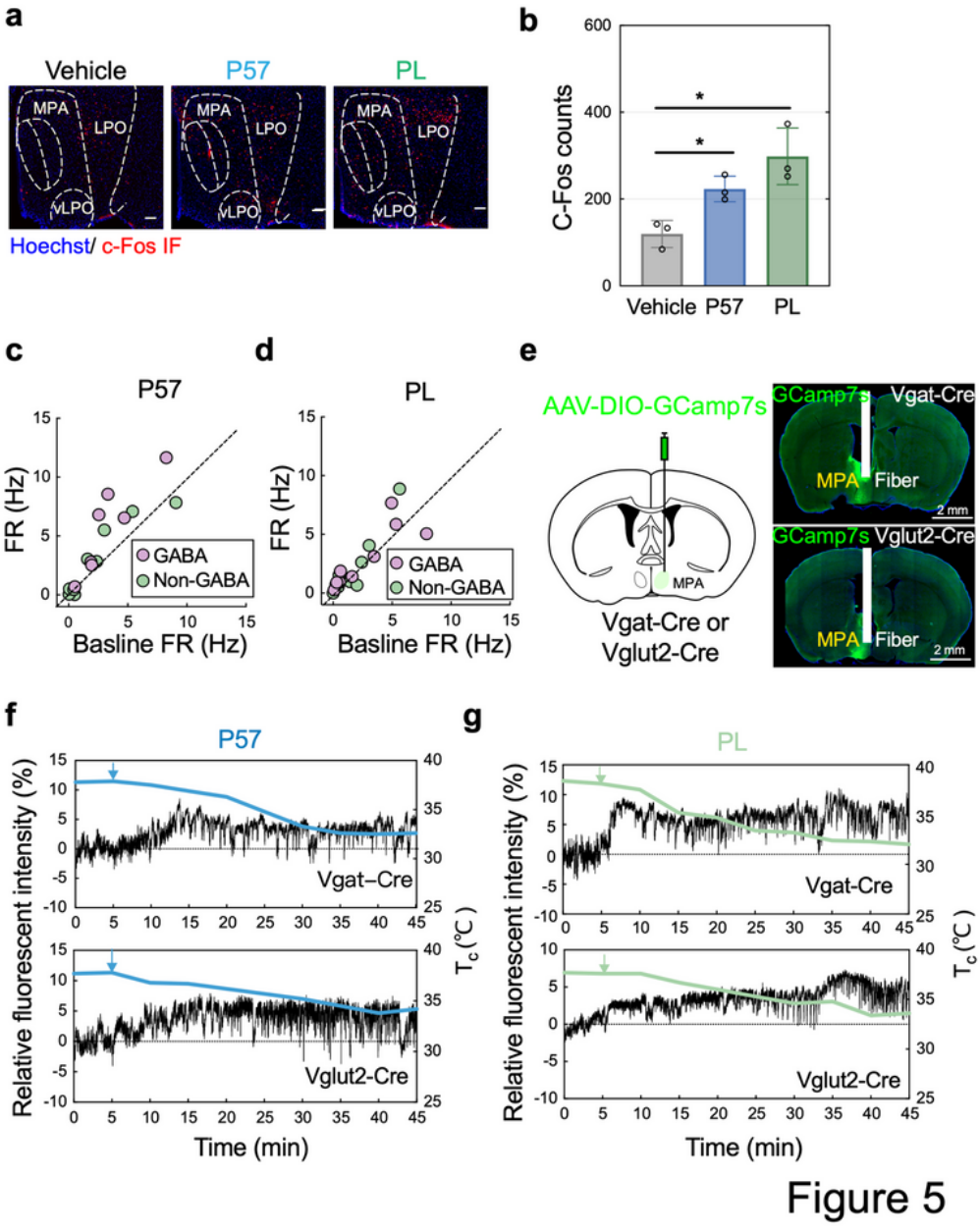

Figure 5

Figure 5

P57 and PL activate neurons in MPA to induce hypothermia. a, Brain sections containing POA immunostained with a neuronal activation marker (c-Fos) 160 min after intraperitoneal injection of vehicle, P57 (25.0 mg/kg) or PL (300.0 mg/kg) (representative of n = 3 mice). Scale bars, 100 μm. The dashed white lines indicate boundaries between subregions. LPO, lateral preoptic nucleus; vLPO, ventrolateral preoptic nucleus. **b,** Quantification of c-Fos-positive neurons in the MPA of each group of (a), mean (n = 3) ± s.d. Dots represent the raw values in each group. The P values compared with vehicle group are calculated based on student's test. * P 0.05 compared to control group, as determined by student's t test. **c,** Firing frequency of GABAergic (n = 7) and non-GABAergic (n = 10) neurons in MPA after treatment with P57 (2.0 μM). Brain slices were prepared from $Vgat^{Cre/-}$; Ai14 mice. Pink dots represent the raw values in GABAergic neurons, green dots represent the raw values in non-GABAergic neurons. **d,** Firing frequency of GABAergic (n = 9) and non-GABAergic (n = 9) neurons in MPA after treatment with PL (10.0 μM). **e,** Schematic showing the injection of AAV2/9-hSyn-DIO-jGCaMP7s-WPRE-pA into the MPA (left) and coronal brain sections showing jGCaMP7s specifically expressed in GABAergic (upper right) or glutamatergic neurons (lower right) in MPA and the location of optical fiber (right). Scale bars, 2 mm. **f, g,** Recording sessions in Vgat-Cre and Vglut2-Cre mice showing T_c and the normalized jGCaMP7s signal. Relative fluorescent intensity is calculated by dividing the smoothed calcium-dependent jGCaMP7s signal with the Ca^{2+}-independent scaled fit. **f,** Example 45-min trace spanning before and after intraperitoneal injection of P57 (25.0 mg/kg) (representative of n = 4 mice). **g,** Example 45-min trace spanning before and after intraperitoneal injection of PL (300.0 mg/kg) (representative of n = 3 mice).

Supplementary Files

This is a list of supplementary files associated with this preprint. Click to download.

- NC202242supplementary.docx